Characterization of the main component of equal width welded I-beam-to-RHS-column connections

Carlos López-Colina*[1], Miguel A. Serrano[1], Miguel Lozano[1], Fernando L. Gayarre[1] Jesús M. Suárez[1], Tim Wilkinson[2]

[1]*Department of Construction and Manufacturing Engineering, University of Oviedo, Building DO7, Pedro Puig Adam St. 33204 Gijón/Xixón, Spain*
[2]*School of Civil Engineering, University of Sydney, J05 Civil Engineering Building, Shepherd St, Darlington NSW 2006, Australia*

Abstract. The present paper tries to contribute fill the gap of application of the component method to tubular connections. For this purpose, one typical joint configuration in which just one component can be considered as active has been studied. These joints were selected as symmetrically loaded welded connections in which the beam width was the same as the column width. This focused the study on the component 'side walls of rectangular hollow sections (RHS) in tension/compression'. It should be one of the main components to be considered in welded unstiffened joints between I beams and RHS columns.
Many experimental tests on double-sided I-beam-to-RHS-column joint with a width ratio 1 have been carried out by the authors and a finite element (FE) model was validated with their results. Then, some different analytical approaches for the component stiffness and strength have been assessed. Finally, the stiffness proposals have been compared with some FE simulations on I-beam-to-RHS-column joints. This work finally proposes the most adequate equations that were found for the stiffness and strength characterization of the component 'side walls of RHS in tension/compression' to be applied in a further unified global proposal for the application of the component method to RHS.

Keywords: connections; component method; stiffness; side walls; RHS

1. Introduction

Many recent advances in the understanding of the behavior of steel structures involves the joint behavior characterization in terms of strength, stiffness and rotation capacity. Higher level analysis and design requires the use of the semi-rigid characteristics of connections rather than the traditional simplified view of rigid or pinned joints. The most common and extended analytical method for the practical evaluation of the joint properties by practitioners is the so-called component method. This procedure divides the connection into different parts or components with their own strength (resistance) and stiffness (force/displacement or moment/rotation ratio). The components are then assembled as a group of springs to obtain the moment resistance and the rotational stiffness of the complete joint. However, this method requires equations that should be able to provide reasonable accurate predictions of the main characteristics (strength and stiffness) of each individual component. These expressions are presented in codes for joints between conventional I and H profiles (Eurocode 2005a). Recent research continues to fill gaps in the knowledge or improve predictions of component behavior such as: fire conditions (Ramli Sulong *et al.* 2010), ductility assessment (Girão Coelho *et al*. 2006), minor axis connections (Kozlowski 2016) or even attempts of general optimization (Chen *et al.* 2017). There is much less research in and application of the component method for hollow sections. (Siong *et al.* 2016).

The most important design guides on hollow sections (Wardenier *et al.* 2010) and hollow section column connections (Kurobane *et al.* 2005) indicate that predicting the stiffness of beam-to-RHS tubular column joints is still not possible with an analytical method, and that limited experimental and FEM moment-rotation curves can be found, such as those by Lu (1997).

More recent research into the component method for tubular joints has been made by Weynand et al. (2015) and Jaspart and Weynand (2015). However, there is still a lack of knowledge in the stiffness characterization of many components.

Some current research trends in this field of component method for RHS are focused on components for bolted connections (Pittrakos and Tizani 2015) and elevated temperatures (Leong Siong *et al.* 2016). Conventional bolts are often not practical for hollow section connections, and some type of blind bolting is necessary (Barnett *et al.* 2001). Since most of these systems are

*Corresponding author, Ph.D. Professor
E-mail: lopezpcarlos@uniovi.es
[a]Ph.D. Professor
[b]M.Sc. Student
[c]Ph.D. Professor
[d]Ph.D. Professor
[e]Ph.D. Professor

expensive or patented, welded I-beam-to-RHS-column connections are still very common. Nevertheless, the research on blind bolted connections has not focused on the component method to characterize the complete joints (Hadianfar and Ranhema 2010), including the ones involving composite slabs (Eslami and Namba 2016) or composite columns (Prabhavathy and Knight 2006). There are some exceptions, but they are concentrated on the strength of specific configurations rather than the stiffness (Quin *et al.* 2015)

For I-beam-to-RHS-column connection is considered, there is a lack of design equations for the components of the RHS column, mainly for their stiffness characterization. The most recent efforts within this subject are focused on the front face of the RHS column in bolted connections (Wang and Park 2011).

According to the statements presented above and considering the inherent difficulties to the bolting process when hollow sections are used, the interest on both the stiffness and the strength characterization of the most important components in directly welded joints between I beams and RHS columns is clear.

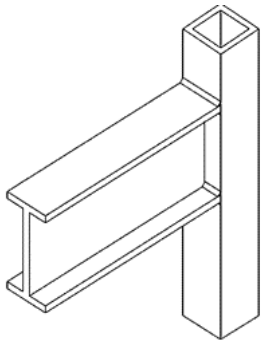

(a) I-RHS joint with $\beta=1$

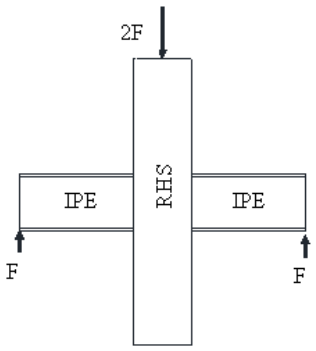

(b) Double sided connection with opposite bending moments

Fig. 1 Description of the selected joint to be studied

When the stiffness of a welded beam-to-column joint involving RHS as a column is considered, its characterization cannot be currently carried out by applying the component method. In addition, the simplest way to obtain a relatively high stiffness value in these welded connections is to design them with a β ratio (beam width/column width) equal or almost equal to *1* (Kurobane *et al.*(2005) as per Fig.1.a. The behavior of these equal-width beam-column joints can be easily simplified through three components: column web under shear, side walls under compression and side walls under tension.

The connections in this study will be double sided I-beam-to-RHS-column with equal and opposite bending moments in the beams. Since this configuration does not cause shear force in the column side walls, the stiffness characterization of the corresponding component is not necessary. The simplest loading arrangement for this type of connections is presented in Fig 1.b.

When the connection of Fig.1.b is considered, the assembly of the lateral faces of the RHS column under tension and under compression (Fig 2.a) through a system of two parallel springs (Fig 2.b) is enough to obtain the rotational stiffness of the beam-to-column joint. The lever arm ($z=h_b-t_f$) is the distance between the centres of the flanges (beam depth less flange thickness). Therefore, if the hypothesis equal stiffness for the component under tension and under compression (K) is assumed, the initial rotational stiffness of the joint can be calculated as $S_{ini}=Kz^2/2$. If the traditional formulation that calculate the stiffness of the

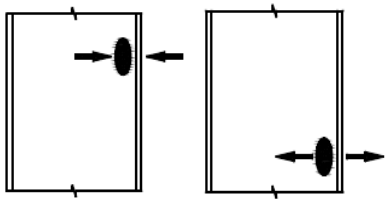

(a) Studied component

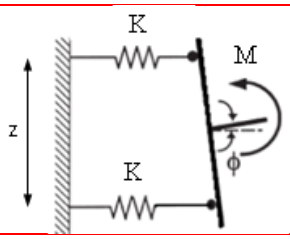

(b) Spring model

Fig. 2 Description of the selected component and the component model

component K from a stiffness coefficient k as $K=k\cdot E$ is considered, the previous expression can be expressed as $S_{ini}=kEz^2/2$.

The strength of the weakest component of the assembly gives the moment resistance of the whole joint by multiplying it by the lever arm (z). If the same steel component subjected to tension or to compression is assumed to have equal or less resistance when compressed because the possibility of some instability effects, the moment resistance of the proposed joint would be $M_R=F_R\cdot z$, being F_R the resistance of the side walls under compression.

Some work was previously carried out by the authors in order to assess the strength and stiffness of the isolated component under ambient and high temperature (López-Colina *et al.* 2010, 2011, 2014). They have been based on the adaptation to this specific component of previous proposals that were initially created either for complete joints (Eurocode 2005a, Yu 1997) or

for the web of open columns (Eurocode 3). Some of them have been provisionally proposed by the CIDECT (Weynand *et al.* 2015) for the improvement of the Eurocode 3-1.8 by extending the component method to hollow section joints.

However, the proposed equations for stiffness and strength of lateral faces of RHS in welded joints summarized by the authors in 2014 (López-Colina *et al.* 2014) have been only validated against some finite element simulations at high temperature and they were models consisting exclusively of plate-to-RHS joints. In addition, the differences between the FE model and the analytical proposal (primarily the stiffness), lead the authors to continue the work on complete beam-to-column joints and including new experimental tests. Following this path, a new (particularly for stiffness) and more reliable proposal is presented in this article for the complete characterization of the component 'lateral faces of RHS'. The complete application of the component method to welded beam-RHS column joints is also checked within this work.

2. Experimental and numerical work

2.1 Experimental tests

Twelve double sided connections were tested according to the loading arrangement presented in Fig. 1.b. The beams were IPE200 and IPE300 and the columns were four different cold formed RHS. All specimens had equal width beam and columns ($\beta=1$). This ensured that the only variable that significantly influenced the joint stiffness would be the lateral faces under tension and under compression. The bottom end of the column was free (see Fig. 1.b). This loading method for double side beam-to-column connection with equal moments is common when the web panel under shear or the effect of the column compression on the joint behaviour are not being investigated (Lu, 1997). It was not necessary to restrain the out-of-plane displacements since the load and supports were applied carefully and taking care of the symmetry to avoid torsional distorting effects. The complete experimental set of connections is described in table 1.

The nominal and measured dimensions are presented (in mm), as well as the main material properties (in MPa). In this table h refers to depth, b to width, t to thickness, a to the weld throat and L to the distance between beam supports. Subscript 0 refers to the RHS column, subscript b refers to the IPE beam and subscripts f and w refer to flange and web respectively. The material properties that are presented in this table were obtained from coupons taken from the faces of the RHS (f_{y0}, ultimate stress f_{u0} and Young's Modulus E_0) and from the flanges of the IPE beam (yield limit f_{yb}).

In tests 1 to 3 the joint rotation was indirectly obtained from the actuator displacement, by considering in this calculation the elastic deflection of a cantilever beam and the shortening of the upper half of the column. The Aramis 5M digital image correlation equipment (Fig. 3) was used in tests 4 to 12 to directly measure the joint rotation. With this sophisticated device, it was possible to measure 3D displacements without having contact with the specimen and then, to synchronize the recorded values with the load applied by the hydraulic jack. Displacements or strains can be measured in all the points included in the area of interest (Fig. 4) and this was used to obtain the beam rotation through the relative vertical displacement of two points chosen on the beam axis that were close to the column.

Table 1 Experimental set

No	RHS	IPE	h_0 [mm]	b_0 [mm]	t_0 [mm]	h_b [mm]	b_b [mm]	t_{fb} [mm]	t_{wb} [mm]	a_f [mm]	a_w [mm]	f_{y0} [MPa]	f_{u0} [MPa]	E_0 [MPa]	f_{yb} [MPa]	f_{ub} [MPa]	L [mm]
1	150×100×6	200	150.1	100.1	5.66	198.2	102.0	8.50	7.59	4.32	3.85	467.5	532.8	187500	367.5	458.9	975
2	100×100×6	200	100.5	100.3	5.95	199.8	102.0	8.50	7.59	3.72	3.64	488.0	542.7	184000	367.5	458.9	975
3	150×100×4	200	150.1	99.8	3.83	199.8	102.0	8.50	7.59	3.35	3.10	467.5	532.8	193500	367.5	458.9	975
4	250×100×6	200	249.0	100.7	5.94	201.6	101.5	8.52	5.53	4.29	4.19	469.1	558.8	200400	367.5	458.9	1205
5	200×100×6	200	119.8	100.5	5.65	199.9	102.1	8.51	6.38	4.15	3.98	397.0	472.8	198700	367.5	458.9	1135
6	200×100×4	200	199.5	101.5	3.95	198.9	101.3	8.52	5.84	3.80	3.42	396.8	473.0	214100	367.5	458.9	1135
7	150×150×6	300	150.0	149.8	5.82	302.9	151.4	9.84	7.54	5.96	5.51	467.5	532.8	209900	298.5	451.4	1128
8	200×150×6	300	199.5	151.0	5.73	298.0	151.3	9.50	8.06	6.20	5.64	397.0	472.8	212500	298.5	451.4	1129
9	250×150×6	300	250.3	150.0	5.92	298.0	151.6	9.40	8.03	6.38	5.24	438.3	535.0	210100	298.5	451.4	1206
10	250×150×8	300	249.5	152.3	7.92	300.6	150.4	10.0	7.46	6.37	5.25	423.5	523.3	172000	298.5	451.4	1194
11	150×100×4	200	150.1	100.2	3.76	200.0	101.3	8.08	5.67	5.11	4.09	412.0	477.2	201800	354.1	453.2	967
12	200×100×4	200	199.0	102.1	3.73	199.7	101.3	8.08	5.63	4.68	3.74	393.9	502.1	194100	354.1	453.2	1130

Fig. 3 Test rig with Aramis DIC system

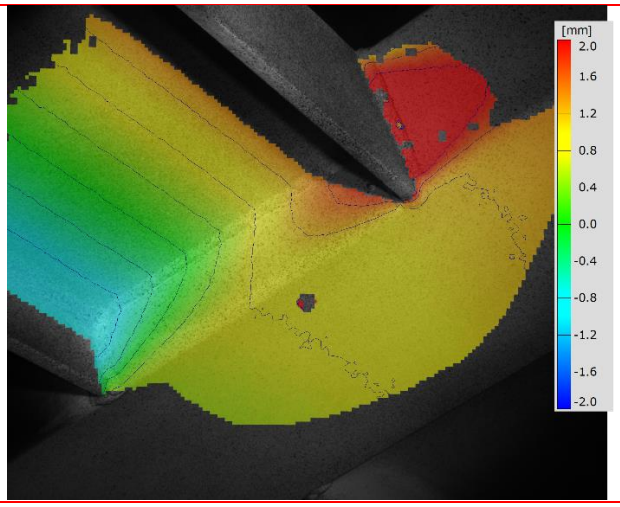

Fig. 4 Displacement measurements with Aramis

2.2 Description of the finite element model

The I beam-to-RHS column tests were reproduced using the FE software ANSYS 17.0 (ANSYS Inc., 2016). Shell elements were used for the members and welds. One half of the joint was modelled by considering the symmetry (Fig.5). The thicknesses of the elements that simulated the weld beads were equal to the weld throat and all the model was created by considering the elements in the middle surface of the plates.

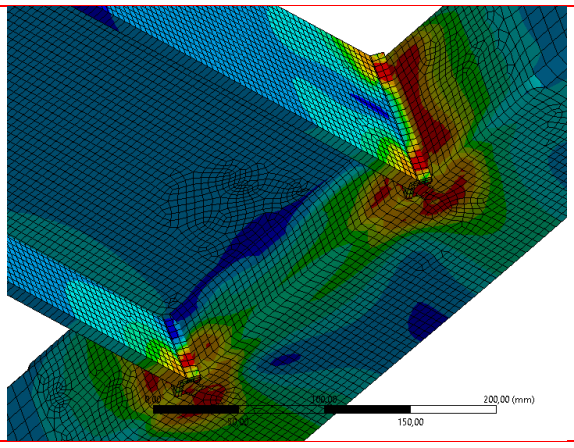

Fig. 5 FE model in ANSYS (Von Mises stresses)

This sort of modelling was previously tested, calibrated and validated by the authors against some experimental tests on I beam-to-RHS column joints published by the University of Delft (Lu, 1997). Additional FEMs with brick and tetrahedral elements were also tried, however no significant differences were found in the results so the increase in complexity and computational time was not justified (Serrano *et al.* 2016).

The material model was considered as elastic-plastic with bilinear isotropic hardening. The slope of the plastic part with strain hardening was set as the Young's Modulus divided by 100, as it is recommended in EC3-1-5 (Eurocode 2006a). This second slope starts at the yield limit, f_y, which was considered homogeneous for the whole section by taking into account the averaged yield limit based on the EC3-1-3 (Eurocode 2006b), but taking the material properties of the faces as an input in the equation, as proposed by the authors in (López-Colina *et al.* 2017). The equation for this transformation is eq. (1):

$$f_y = f_{y0} + 28\frac{t_0^2}{A_0}\left(f_{u0} - f_{y0}\right) \quad (1)$$

Where t_0 is the thickness, A_0 is the area of the cross section and f_{u0} and f_{y0} are the ultimate stress and yield limit of the face of the RHS respectively.

2.3 Validation of the finite element model

Despite the previously mentioned comparison of the finite element model with external experimental tests, an additional validation focused on the rotational stiffness and the moment resistance was performed taking into account the results of the experimental tests described in 3.1. Table 2 shows the comparison between the initial stiffness ($S_{ini,FEM}$) from FEM and initial stiffness ($S_{ini,TST}$) from tests. Only the experimental initial rotational stiffness of tests 4 to 12 was compared with the FEM results, since the indirect calculation of stiffness that could be made for the first three tests was not reliable enough to be considered an accurate source of experimental data. In addition, Table 2 presents the resistances obtained from the FE model ($M_{R,FEM}$) and the ones from the experimental tests ($M_{R,TST}$). The resistances for both FEM and experimental test were obtained by taking either the maximum value from the moment-rotation curve or the moment when the deformation of the component reaches the *3*% of b_0 (Lu 1994). Therefore, the resistances M_R were initially defined in Table 2 by the criterion that was reached first, i.e. the maximum moment or the moment at the *3*%b_0 deformation limit.

Table 2 Validation of the stiffness and resistance from FEM

No	RHS	$S_{ini,FEM}$ [kN·m/rad]	$S_{ini,TST}$ [kN·m/rad]	$D_{if,S}$ [%]	$M_{R,FEM}$ [kN·m]	$M_{R,TST}$ [kN·m]	$D_{if,MR}$ [%]
1	150×100×6	9154	-	-	47.46	44.15	-7.5
2	100×100×6	10046	-	-	48.62	43.87	-10.8
3	150×100×4	6337	-	-	25.67	25.16	-2.0
4	250×100×6	9655	8676	-11.3	44.16	39.70	-11.2
5	200×100×6	8363	8149	-2.6	44.31	35.59	-24.5
6	200×100×4	6546	6363	-2.9	26.59	22.68	-17.2
7	150×150×6	22920	22914	-0.0	92.57	85.10	-8.8
8	200×150×6	21273	21760	2.2	81.76	77.43	-5.6
9	250×150×6	21333	22609	5.6	94.18	91.78	-2.6
10	250×150×8	22535	21496	-4.8	127.00	109.28	-16.2
11	150×100×4	6620	6038	-9.6	28.54	29.98	4.8
12	200×100×4	6239	6020	-3.6	28.42	28.38	-0.1

Despite certain trend to slightly unconservative values (negative values of $D_{if,S}$), for the purpose of this research the results show very good agreement between the model and the experiment when the initial stiffness is compared (Fig. 6). They present an average absolute error of *4.76*% and a standard deviation of *6.22*%. When the moment resistance is compared (see Fig. 7), the average absolute error is *9.29*% and the standard deviation is *12.07*%. Table 2 shows differences over *10*% on the unconservative side in some tests, but these are caused by the cracking and the premature brittle fracture that was observed in most of experimental tests (all tests excepting 7, 9, 11 and 12). As it was stated by Van der Vegte et al. (2010), finite element simulations currently used cannot predict cracking and fracture properly and sophisticated models, such as critical strain or damage criterion, are required. However, this fracture can be observed in the moment-rotation curves presented in Fig. 8. The graph shows only the experimental-FEM comparison for 4 representative tests with cracking and fracture before the *3*%b_0 deformation limit. The other 4 cases that present this type of failure (numbers 1, 2, 3 and 5) have not been represented since they are similar and reach approximately the same ranges of moment resistances.

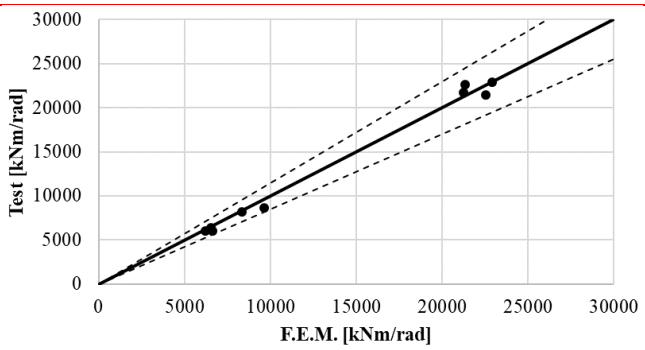

Fig. 6 Comparison of initial stiffness S_{ini} (tests vs FEM)

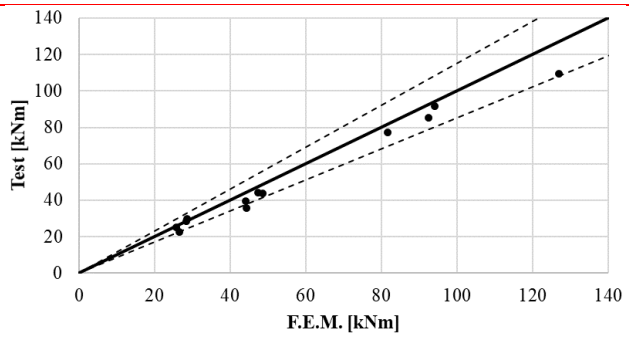

Fig. 7 Comparison of moment resistance M_R (tests vs FEM)

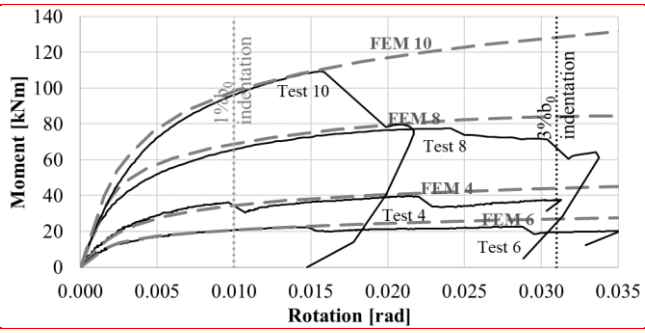

Fig. 8 Some M-θ curves when fracture is observed

Experimental and numerical curves 9 and 11 are presented in Fig. 9. Those obtained from tests 7 and 12 are very similar and their representation would almost overlap the previous ones.

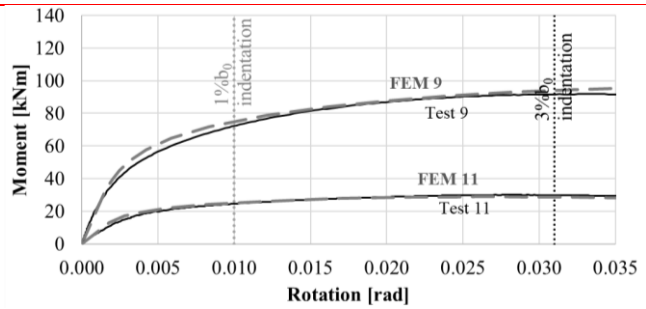

Fig. 9 Some M-θ curves without fracture

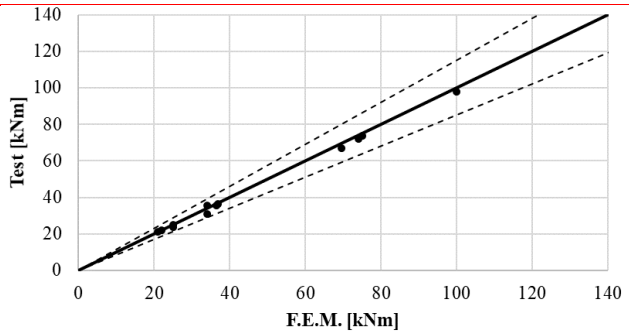

Fig. 10 Comparison of resistance at $1\%b_0$ (tests vs FEM)

Since the finite element model cannot reproduce the cracking and the fracture, the moment resistance at a deformation limit of $1\%b_0$ was also considered as an additional reference value for the validation ($M_{1\%b0}$), giving very good agreement (see Fig. 10) because the average absolute error was *3.04*% and the standard deviation was *4.08*%.

2.4 Extension of the FE model for the stiffness study

The good results obtained in the above presented validation for the initial stiffness leaded to an extension of the finite element model. It was planned as a study in which the influence of main size parameters of the RHS column on the initial stiffness was assessed. Three typical IPE profiles were used (IPE200, IPE240 and IPE300). Since the above stated condition for the present research was that the RHS column should have the same width as the IPE flange, the only parameters that can change in each group of joints associated to each IPE profile are the column depth h_0 and the column wall thickness t_0. Figs. 11 to 13 present graphically the results of initial rotational stiffness (S_{ini}) obtained in the 27 FE simulations that were carried out.

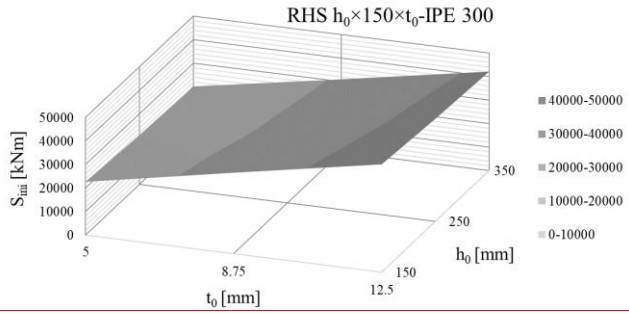

Fig. 11 Response surface of RHS-to-IPE300 joints

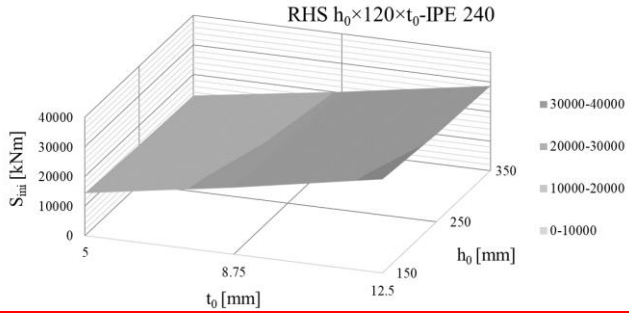

Fig. 12 Response surface of RHS-to-IPE240 joints

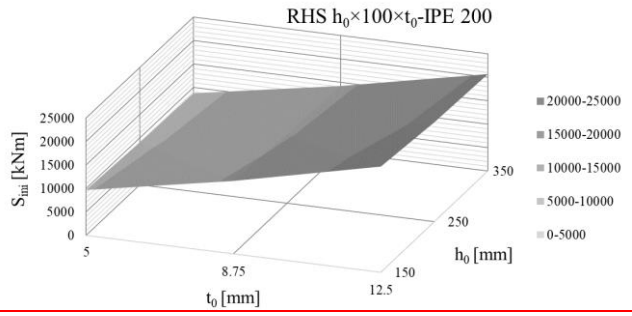

Fig. 13 Response surface of RHS-to-IPE200 joints

The previous graphs show a clear dependence of the stiffness on the RHS thickness t_0 and a slighter dependence on the width of the lateral faces h_0. The rotational stiffness increases with the thickness and decreases when the size of the lateral faces increases.

3. Assessment of different stiffness proposals

Four different analytical and semi-empirical approaches to the stiffness of side walls of RHS (k) have been tested. They are based on the adaptation of different equations proposed initially for the stiffness of the component column web under compression and tension in open profiles. The approaches presented in sub-sections 3.1 and 3.2 were previously considered by the authors (López-Colina *et al.* 2011) as a starting point for the stiffness characterization of the component. In this section they are assessed again with the new FE data and it is confirmed that there is a wide margin for improvement. These better results have been obtained with the proposals presented in sub-sections 3.3 and 3.4.

3.1 Adapted model for I and H profiles

This was the model initially proposed for the component in the study carried out on the lateral faces of RHS under ambient and high temperatures as an isolated component (López-Colina *et al.* 2011, 2014), being essentially the Eurocode proposal for the stiffness of column webs under transverse tension and compression (Eurocode 2005a). Although in those studies it gave reasonable results for the isolated RHS profile under a transverse compression, it was only checked against a FEM with this condition: isolated RHS profile. Therefore, the fact of including welds between a plate (flange) and the RHS was not still considered. In addition, the application to a whole connection was not deeply studied excepting by a partial comparison with two experimental tests taken from the literature. All these factors cause that this equation cannot be accurately applied for this more extensive study on welded beam-to-column joints as it is seen in Fig. 14, that compares the results of initial stiffness of the obtained from the analytical approach and the FE model. These inaccurate results discourage the use of this approach without a substantial change

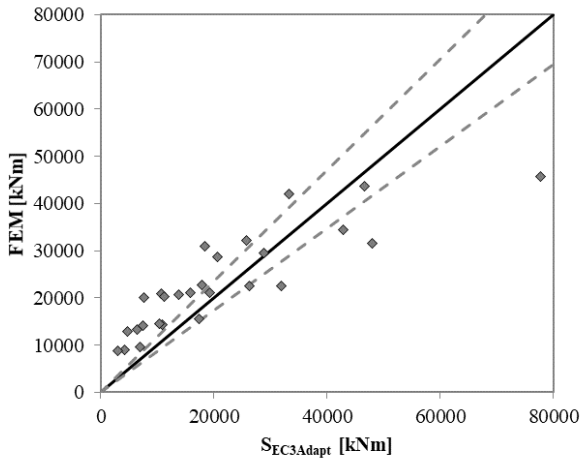

Fig. 14 Comparison adapted EC3 model vs FEM

3.2 Four hinges model

The application of the same 4 hinges model that can be used for resistance (López-Colina *et al.* 2010, 2014) was assessed for the determination of the initial stiffness. However, even optimizing the typical modifier factor that was used to obtain the

effective width of the lateral faces (usually taken as *0.7*) it was impossible to obtain a better approach for the stiffness of the joint than the presented in Fig. 15.

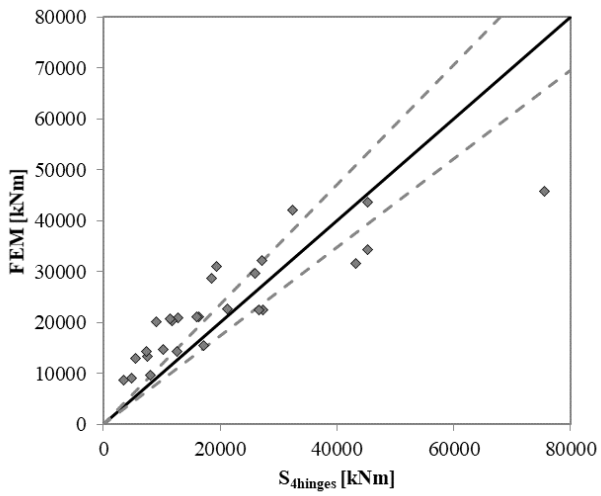

Fig. 15 Comparison 4-hinges model vs FEM

3.3 Adapted empirical model 1

This model is based on the empirical one initially proposed for the stiffness of I and H webs under transverse compression by Aribert *et al.* (1990) by successfully adapting it to RHS. It was originally proposed as a fourth root of the RHS width to depth ratio ($0.45 \cdot t_0 \cdot \sqrt[4]{b_0/h_0}$). However, for RHS profiles, the result for the stiffness coefficient k is better modelled using the eighth root as given in Eq. (2). The results for the initial stiffness of the joint using this approach are presented and compared with FEM results in Fig. 16.

$$k = 0.45 \cdot t_0 \sqrt[8]{\frac{b_0}{h_0}} \quad (2)$$

where t_0, b_0 and h_0 are the dimensions (thickness, width and depth) of the RHS column.

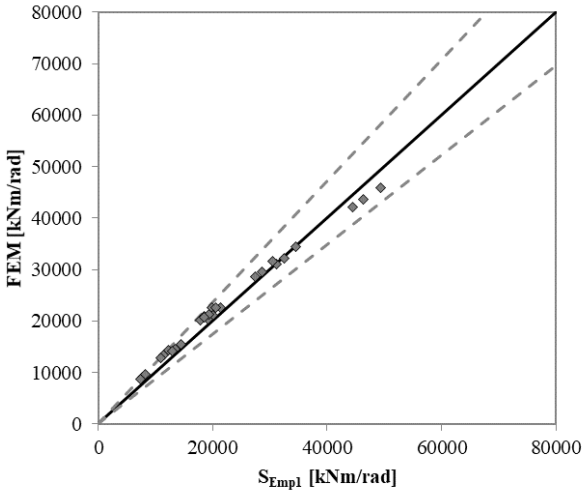

Fig. 16 Comparison empirical model 1 vs FEM

3.3 Adapted empirical model 2

This second empirical model is based on the initially proposed as an enhancement of the one by Aribert *et al*. (1990). It was based on fatigue of I and H sections under transverse load (Aribert *et al.* 2002). It was then designed as a dimensionless fourth root multiplied by the thickness and by a coefficient *0.95*. This model inserted the effective width b_{eff} in the equation. However, it was noticed here that for RHS profiles the most suitable modification is Eq. (3), with an eighth root instead of a fourth one and a coefficient *0.59* instead of *0.95*. The results are presented in Fig. 17.

$$k = 0.59 \cdot t_0 \sqrt[8]{\frac{b_0 \cdot t_0}{b_{\text{eff}} \cdot h_0}} \quad (3)$$

where t_0, b_0 and h_0 are the dimensions (thickness, width and depth) of the RHS column and the effective width is calculated by considering the flange thickness t_f and the weld bead a_f with Eq. (4):

$$b_{\text{eff}} = t_f + 2 \cdot \sqrt{2} \cdot a_f + 5 \cdot t_0 \quad (4)$$

Figures 15 and 16 show clearly the best performance of the equations that were obtained by adapting the empirical ones initially proposed for I and H profiles. The third and fourth proposal present percentage deviations of their results from the FEM of which the means of their absolute values are *8.4*% and *8.2*% respectively for the 27 cases studied. In addition, the maximum deviation from the validated FEM was approximately *15*% in the third proposal and *16*% in the fourth one.

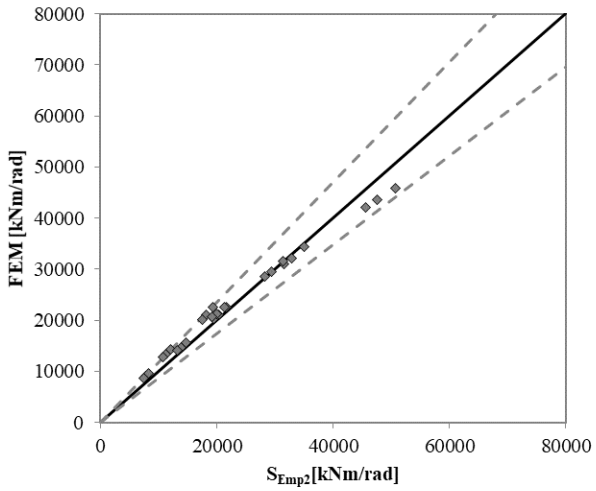

Fig. 17 Comparison empirical model 2 vs FEM

4. Assessment of different resistance proposals

Despite the main necessity of a new component equation for the lateral faces of RHS was centred on stiffness, two previous proposals for the component strength has been tested in order to assess their performance when complete joints are considered.

4.1 Adapted model for transverse plate to RHS joint.

Based on the resistance traditionally considered for a joint between a transverse plate welded to a RHS when they both have the same width (β=1) (Eurocode 2005a), the resistance of the component lateral faces of RHS can be obtained from Eq. (5).

$$F_R = 2 \cdot b_{\text{eff}} \cdot f_y \cdot t_0 \quad (5)$$

where the effective width b_{eff} is given in Eq. (4).

Fig 18 presents the moment resistance (M_R) of the beam-column joints calculated from the component resistance of Eq. (5) compared with the experimental capacities. The mean deviation value for this approach is about *16.5*%.

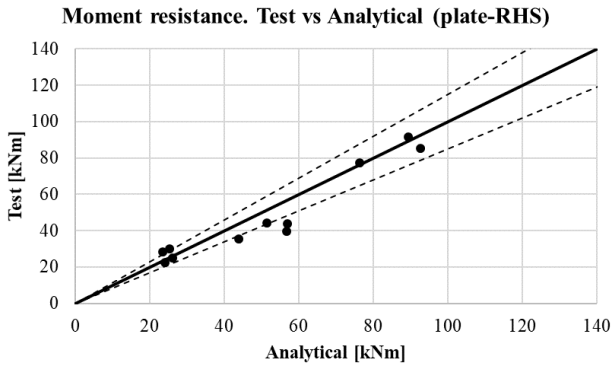

Fig. 18 Comparison of M_R from tests vs plate-RHS model

4.2 4-hinges model with buckling.

The second equation for the resistance of the component lateral faces of RHS (López-Colina et al. 2010) is based on a four-hinges model and considering the reduction caused by buckling in the compression component, using a similar as Yu (1997) for RHS T-joints.

$$F_R = 2 \cdot f_y \cdot t_0 \cdot \chi \cdot \left(t_f + 2 \cdot \sqrt{2} \cdot a_f + 2 \sqrt{\frac{b_0 \cdot t_0}{2 \cdot \chi}} \right) \quad (6)$$

The reduction factor for buckling χ is obtained with the normalized slenderness from the corresponding buckling curve. For the cold formed tubes considered in the experimental program, curve *c* from Eurocode (2005b) can be proposed.

Fig. 19 shows the comparison between the moment resistances M_R obtained in experimental tests and their corresponding values calculated through the component resistance of Eq. (6) as $M_R = F_R \cdot z$. The mean deviation value for this analytical approach is about *17*%.

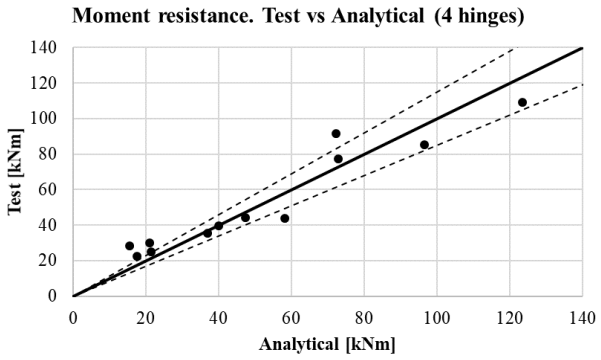

Fig. 19 Comparison of M_R from tests vs 4-hinges model

5. Summary and conclusions

This paper has presented experimental and finite element results and comparison of stiffness and resistance of I- beam to RHS connections for use in the component method. The following conclusions can be made:

- The experimental apparatus that was proposed allowed a digital and precise analysis of images that avoided the inherent difficulties of the LVDT-based arrangements.
- The finite element modelling proposed previously for welded joints between I beams and RHS columns was validated again against the new experimental work, confirming good agreement with the experimental stiffness.
- The cracking and fracture that appeared in many welds cannot be reproduced with the simplified finite element model.
- Despite the previous limitation, if the curves until the fracture failure are considered or the moment resistance at a component deformation of *1*%b_0 (serviceability limit) is taken into account, very good agreement is obtained.
- The extension of the finite element model showed that the thickness of the RHS has higher influence on the stiffness of their side walls than other parameters.
- The two semi-analytical models that were previously proposed through an adaptation of the EC3 equations for the stiffness of the column web component and by adapting the four-hinges model did not give good agreement with the validated FEM.
- The two simple empirical equations for I and H profiles led to good results for the component stiffness.
- "Empirical model 1" for stiffness is recommend for practical design purposes due to closer prediction and simplicity.
- The experiments showed that cracking and fracture in lateral welds of beam flanges is a common failure at component deformations between *1*%b_0 and *3*%b_0.
- As a practical fabrication recommendation, special care should be taken when lateral welds between of beam flanges are carried out in equal width welded I-beam to RHS columns.

- The fracture failures cause some variability in resistance results and make difficult to obtain a very accurate analytical model for the component strength.
- Two resistance prediction equations have been and both can be useful for design purposes.
- The reasonable results and simplicity of the adapted model for transverse plate to RHS are reasons enough to confirm its worth as resistance equation for the studied component.

6. Acknowledgments

This research was supported by the Spanish R&D Nat. Program as a part of project BIA2013-43177-P and it was also supported, reviewed and approved by the Committee for International Development and Education on Construction of Tubular structures (CIDECT), as part of project 5CE.

7. References

ANSYS, Inc. (2016), *ANSYS 17.0 Release notes*, ANSYS, Canonsburg, PA, USA.

Aribert, J.M., Lachal, A., Moheissen, M. (1990), "Modelling and experimental investigation of plastic resistance and local buckling of H or I steel sections submitted to concentrated or partially distributed loading", *Contact Loading and Local Effects in Thin-walled Plated and Shell Structures. IUTAM Symposium*, Prague, September.

Aribert, J.M., Younes, I., Lachal A. (2002) "Low-cycle fatigue of steel connections subjected to a transverse concentrated load: experimental investigation and practical formulation", *Proceedings of 3rd European Conference on Steel and Composite Structures*, Coimbra, September.

Barnett, T.C., Tizani, W. and Nethercot, D.A. (2001), "The practice of blind bolting connections to structural hollow sections: a review", *Steel and Composite Structures*, **1**(1), 1-16.

Chen, S., Pan, J., Yuan, H., Xie, Z., Wang, Z. and Dong, X. (2017) "Mechanical behavior investigation of steel connections using a modified component method", *Steel and Composite Structures*, **25**(1), 117-126.

Eslami, M. and Namba, H. (2016), "Rotation capacity of composite beam connected to RHS column, experimental test results", *Steel and Composite Structures*, **22**(1), 141-159.

Eurocode (2005a), *Design of Steel Structures*. Part 1-8: Design of Joints, European Committee for Standardization; Brussels, Belgium.

Eurocode (2005b), *Design of Steel Structures*. Part 1-1: General Rules and Rules for Buildings, European Committee for Standardization; Brussels, Belgium.

Eurocode (2006a), *Design of Steel Structures*. Part 1-5: Plated Structural Elements, European Committee for Standardization; Brussels, Belgium.

Eurocode (2006b), *Design of Steel Structures*. Part 1-3: General Rules. Supplementary Rules for Cold-Formed members and Sheeting, European Committee for Standardization, Brussels, Belgium.

Girao Coelho, A.M., Simoes da Silva, L., Bijlaard, F.S. (2006), "Ductility analysis of bolted extended end plate beam-to-column connections in the framework of the component method", *Steel and Composite Structures*, **6**(1), 33-53.

Hadianfar, M.A., Rahnema, H. (2010), "Effects of RHS face deformation on the rigidity of beam-column connection", *Steel and Composite Structures*, **10**(6), 491-502

Jaspart, J.P., Weynand, K. (2015) "Design of hollow section joints using the component method", *Proceedings of 15th International Symposium on Tubular Structures*, Rio de Janeiro, May.

Kurobane, Y., Packer, J.A., Wardenier, J., Yeomans, N. (2005), *Design guide 9 for structural hollow section column connections*, TÜV-Verlag GmbH, Cologne, Germany.

Kozlowski, A. (2016) "Component method model for predicting the moment resistance, stiffness and rotation capacity of minor axis composite seat and web site plate joints", *Steel and Composite Structures*, **20**(3), 469-486.

Leong Siong, H.; Ramli Sulong, N.H. and Jameel, M. (2016), "Bolted connections to tubular columns at ambient and elevated temperatures - a review", *Steel and Composite Structures*, **21**(2), 303-321.

López-Colina, C., Serrano, M.A., Gayarre, F.L., Suárez, F.J. (2010), "Resistance of the component 'lateral faces of RHS' at high temperature", *Engineering Structures*, **32**(4), 1133-1139.

López-Colina, C., Serrano, M.A., Gayarre, F.L., del Coz, J.J. (2011), "Stiffness of the component 'lateral faces of RHS' at high temperature", *Journal of Constructional Steel Research*, **67**(12), 1835-1842.

López-Colina, C., Serrano, M.A., Gayarre, F.L., González, J. (2014), "The component 'lateral faces of RHS' under compression at ambient and high temperature", *International Journal of Steel Structures*, **14**(1), 13-22.

López-Colina, C., Serrano, M.A., Lozano, M., Gayarre, F.L., Suárez, J. (2017), "Simplified Models for the Material Characterization of Cold-Formed RHS", *Materials* **10**(9), 1043.

Lu, L.H., de Winkel, G.D., Yu, Y., Wardenier, J. (1997) "Deformation limit for the ultimate strength of hollow section joints", *Proceedings of 6th International Symposium on Tubular Structures*, Melbourne, December.

Lu, L.H. (1997), "The static strength of I-beam to rectangular hollow section column connections", PhD Dissertation, Delft University of Technology, Delft.

Prabhavathy, A. and Knight, G.M. (2006), "Behaviour of cold-formed steel concrete infilled RHS connections and frames", *Steel and Composite Structures*, **6**(1) 71-85.

Quin, Y., Chen, Z. and Rong, B. (2015) "Component-based mechanical models for concrete-filled RHS connections with Diaphragms under bending moment", *Advances in Structural Engineering*, **18**(8), 1241-1256.

Ramli Sulong, N.H., Elghazouli, A.Y., Izzuddin, B.A. and Ajit, N. (2010) "Modelling of beam-to-column connections at elevated temperature using the component method", *Steel and Composite Structures*, **10**(1) 23-43.

Serrano, M.A., López-Colina, C., González, J., Gayarre, F.L. (2016) "A simplified simulation of welded I beam-to-RHS column joints", *International Journal of Steel Structures* **16**(4), 1095-1105.

Van der Vegte, G.J., Wardenier, J., Puthli R.S. (2010) "FE analysis for welded hollow section joints and bolted joints", *Proceedings of the Institution of Civil Engineers - Structures and Buildings* **163**(6), 427-437.

Wang, Y.C. and Park, A.Y. (2011), "Development of component stiffness equations for bolted connections to RHS columns", *Journal of Constructional Steel Research*, **70**, 137-152

Wardenier, J., Packer, J.A., Zhao, X.L., van der Vegte, G.J. (2010) *Hollow Sections in Structural Applications*, (2nd Edition), CIDECT, Geneva, Switzerland.

Weynand, K., Jaspart, J.P., Demonceau, J.F., Zhang, L., (2015), "Component method for tubular joints" Draft Final Report No. 16F-3/15; Comité International pour le Développement et l´Etude de la Construction Tubulaire, Liège.

Yu, Y. (1997), "The static strength of uniplanar and multiplanar connections in rectangular hollow sections", PhD Dissertation, Delft University of Technology, Delft.